INTERNATIONAL JOURNAL FOR NUMERICAL METHODS IN FLUIDS
Int. J. Numer. Meth. Fluids 2008; **56**:453–465
Published online 19 June 2007 in Wiley InterScience (www.interscience.wiley.com). DOI: 10.1002/fld.1539

Role of the inclination of an inverted-V upper plate on the heat and flow behavior of trapped gases in a modified Rayleigh–Bénard cavity

El Hassan Ridouane[1,*,†], Antonio Campo[1] and Jane Y. Chang[2]

[1]*Department of Mechanical Engineering, The University of Vermont, Burlington, VT 05405, U.S.A.*
[2]*Department of Applied Statistics and Operation Research, Bowling Green State University, Bowling Green, OH 43403, U.S.A.*

SUMMARY

Thermal buoyant air inside a modified Rayleigh–Bénard (RB) cavity bounded by a lower flat plate and an inverted-V upper plate has been investigated numerically using the finite-volume method. The second-order-accurate QUICK and SIMPLE schemes were used for the discretization of the convective terms and the pressure–velocity coupling in the set of conservation equations, respectively. The problem under study is controlled by two parameters: (1) the Rayleigh number ranging from 10^3 to 10^6 and (2) the relative height of the vertical sidewalls d. In reference to the latter, it varies from one limiting case corresponding to the standard RB cavity (a rectangle with $d = 1$) to another limiting case represented by an isosceles triangular cavity where $d = 0$. The numerical results for the velocity and temperature fields are presented in terms of streamlines, isotherms, local and mean heat fluxes. An additional effort was devoted to determine the critical *Ra* values characterizing the transition from symmetrical to asymmetrical buoyant airflow responsive to incremental changes in *Ra*. For purposes of engineering design, a general correlation equation for the Nusselt number in terms of the pertinent *Ra* and *d* was constructed using nonlinear multiple regression theory. Copyright © 2007 John Wiley & Sons, Ltd.

Received 13 December 2006; Revised 23 April 2007; Accepted 27 April 2007

KEY WORDS: modified Rayleigh–Bénard cavity; finite volume method; transition; heat transfer enhancement

1. INTRODUCTION

The standard Rayleigh–Bénard cavity (hereafter the RB cavity) is considered as a classic problem in fluid mechanics and thermal convection [1, 2]. A standard RB cavity is defined as an enclosed space long and wide in the horizontal direction which is bounded by two large horizontal plates

*Correspondence to: El Hassan Ridouane, Department of Mechanical Engineering, The University of Vermont, Burlington, VT 05405, U.S.A.
†E-mail: eridouan@cems.uvm.edu

held at uniform temperatures, the lower plate being at a temperature T_H higher than the upper plate at a temperature T_C. The fluid medium is normally a single-phase Newtonian liquid or a pure gas.

The physics of fluids stipulates that the heat transport by natural convection in a RB cavity is conformed by two modes [1, 2]. The first mode is prototypical of molecular conduction of heat in the quiescent fluid layer that separates the two opposing horizontal plates. In this mode, the buoyant forces are weak and cannot overcome the viscous forces creating an imbalance of forces. Consequently, the molecular conduction mode is described by a linear temperature variation so that the transfer of heat across the quiescent fluid layer is portrayed by a unitary Nusselt number, $Nu = 1$. This plain pattern remains unaltered as Ra increases up to the attainment of a critical Rayleigh number, $Ra_C \cong 1708$ [1, 2]. When the temperature differential at the horizontal walls $T_H - T_C$ is raised gradually, the buoyancy forces are intensified, and eventually outweigh the viscous forces. This state of affairs is governed by $Ra > Ra_C$, and as a result the fluid circulation becomes stronger. The fluid movement coupled with molecular heat conduction brings with it a second mode of heat transport [1, 2]. This situation is connected to moderate-to-large values of the Ra numbers, which are confined to the Ra sub-interval $1708 < Ra < 3.2 \times 10^5$. Within this ample sub-interval, the fluid possesses laminar motion and takes the form of 2-D regularly spaced counter-rotating roll cells of square cross section. These cells are traditionally recognized as Bénard cells in honour of Bénard [3] who first observed this singular phenomenon in 1900. Further increases in the temperature differential at the horizontal walls $T_H - T_C$ exceed the upper limit of $Ra = 3.2 \times 10^5$, carrying with it 2-D roll cells that break apart and immediately form a new 3-D cells which appear hexagonal in shape when viewed from above. Whenever $Ra \gg 3.2 \times 10^5$, the natural convective flow energizes even further, the number of 3-D cells multiply, turn narrower and the flow becomes oscillatory turbulent. Eventually, the 3-D cells disappear.

From the brief narration, it is apparent that the heat transport in a RB cavity responds to: (a) molecular conduction for $Ra < 1708$; (b) laminar natural convection for $Ra > 1708$; and (c) turbulent natural convection for $Ra \gg 1708$. A simple WEB literature search reveals a superabundance of publications on thermal convection related to the standard RB cavity.

As expected, heat transfer enhancement in RB cavities turns out to be difficult because of the low fluid velocities that are induced by gravitational flows. Owing to this adverse effect, it is of fundamental and practical interest to explore schemes for augmenting heat transfer in RB cavities. In this regard, Hitt and Campo [4] attached conductive fins to the bottom plate of a RB cavity with encouraging Nu results. Thereby, the aim of the present paper is to explore the heat/flow implications of inclining the upper cold plate of a standard RB cavity with a goal at increasing heat transfer rates. Despite that the authors Lam *et al.* [5], Peric [6], Sadat and Salagnac [7], and Moukalled and Acharya [8, 9] have tackled thermal convection in trapezoidal enclosures, none of these works relate to the configuration under investigation in this study.

2. PROBLEM FORMULATION

A schematic diagram of the modified RB cavity for the case under study appears in Figure 1. The cavity domain is bounded from below by a flat plate, from above by an inverted-V plate with variable inclination angle, and from the sides by two vertical insulated boundaries. The horizontal and vertical coordinates are x, y. The dimensions of the modified RB cavity in Figure 1 are stated as follows: base $L = 2H$, maximum height H, and variable height of the insulated sidewalls d'. The fluid medium is air. The dimension perpendicular to the sketch plane is relatively long, so that

DOI: 10.1002/fld

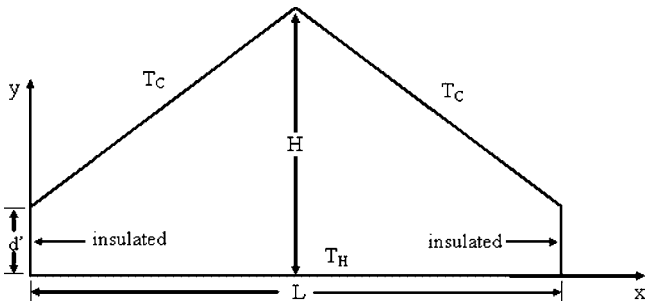

Figure 1. Modified Rayleigh–Bénard cavity with a lower flat plate and an inverted-V upper plate.

the air circulation has 2-D motion. The airflow is governed by the 2-D unsteady coupled system of mass, momentum, and energy conservation equations with the following restrictions: laminar flow, constant thermophysical properties, Boussinesq approximation, and Newtonian fluid. These equations are

$$\frac{\partial u}{\partial x}+\frac{\partial v}{\partial y}=0 \tag{1}$$

$$\frac{\partial u}{\partial t}+u\frac{\partial u}{\partial x}+v\frac{\partial u}{\partial y}=-\frac{1}{\rho}\frac{\partial p}{\partial x}+\upsilon\left(\frac{\partial^2 u}{\partial^2 x}+\frac{\partial^2 u}{\partial^2 y}\right) \tag{2}$$

$$\frac{\partial v}{\partial t}+u\frac{\partial v}{\partial x}+v\frac{\partial v}{\partial y}=-\frac{1}{\rho}\frac{\partial p}{\partial y}+\upsilon\left(\frac{\partial^2 v}{\partial^2 x}+\frac{\partial^2 v}{\partial^2 y}\right)+g\beta(T-T_r) \tag{3}$$

$$\frac{\partial T}{\partial t}+c_P u\frac{\partial T}{\partial x}+c_P v\frac{\partial T}{\partial y}=\frac{k}{\rho}\left(\frac{\partial^2 T}{\partial^2 x}+\frac{\partial^2 T}{\partial^2 y}\right) \tag{4}$$

The velocity boundary conditions rest on the basic assumptions: (a) the solid boundaries are rigid and impermeable; and (b) the air does not slip at the fluid/solid interfaces, i.e. $u=v=0$. The temperature boundary conditions imply prescribed $T_{\mathrm{H}}=313\,\mathrm{K}$ at the bottom hot plate, prescribed $T_{\mathrm{C}}=287\,\mathrm{K}$ at the two upper symmetrically inclined cold plates, and null temperature gradient $\partial T/\partial x$ at the two bounding insulated sidewalls. The initial condition is set at T_{C}.

3. NUMERICAL COMPUTATIONAL PROCEDURE

The computational domain is constructed coincident with the physical domain forming the modified RB cavity. All computations were done for a fixed aspect ration of $H/L=2$. The relative height $d=d'/H$ of the insulated sidewalls is contained in the interval 0 (for an isosceles triangle) $<d<1$ (for a standard RB cavity). Representative Rayleigh numbers ranging from a low $Ra=10^3$ to a high 10^6 are employed to secure laminar conditions.

The computational domain has been constructed using quadrilateral elements. Moreover, the regions near the solid surfaces (plates and sidewalls) are meshed with fine grids to resolve the high

DOI: 10.1002/fld

Table I. Sensitivity of the grid density in terms of the mean Nusselt number for the case of $d = 0.125$ and $Ra = 10^6$.

Grid size	*Nu*
30 000	9.64
40 000	9.87
50 000	10.02
57 000	10.43
70 000	10.54

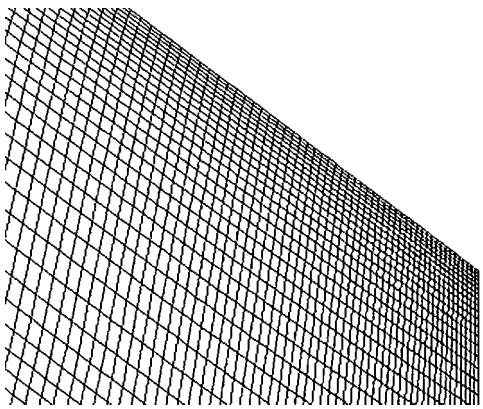

Figure 2. Portion of the computational grid showing the distribution of elements within the right corner between the vertical sidewall and the inclined plate of the modified RB cavity with $d = 0.25$.

velocity and temperature gradients that normally occur there. First, for the subset of modified RB cavities with $0 \leqslant d \leqslant 0.75$, a total of 57 000 finite-volume quadrilateral elements are employed to attain grid-independent solutions. Second, for the extreme standard RB cavity with $d = 1$, a total of 20 000 quadrilateral elements were utilized. The process of mesh refinement is repeated progressively until insignificant velocity and temperature changes are guaranteed at all computational domain locations. The numerical uncertainty of the two velocity components u and v should be less than 2%, while the local heat flux q stays around 5%. The items in Table I indicate how the mean Nusselt number converges with the sequential grid refinements for the case of $d = 0.125$ and $Ra = 10^6$. For purposes of visualization, a portion of the computational grid corresponding to the right corner of the modified RB cavity with $d = 0.25$ is shown in Figure 2.

To perform the numerical computations of the velocity and temperature fields $u(x, y)$, $v(x, y)$ and $T(x, y)$ satisfying the applicable velocity and temperature boundary conditions stated before, the governing equations (1)–(4) are solved using the finite-volume method. In this context, the fully implicit discretization approach was used for discretizing the transient equations on the grounds of its superior stability. The QUICK scheme was used for the discretization of momentum and energy conservation equations. A second-order body-force-weighted scheme was utilized in the pressure discretization and the SIMPLE scheme was employed in the pressure–velocity coupling [10].

DOI: 10.1002/fld

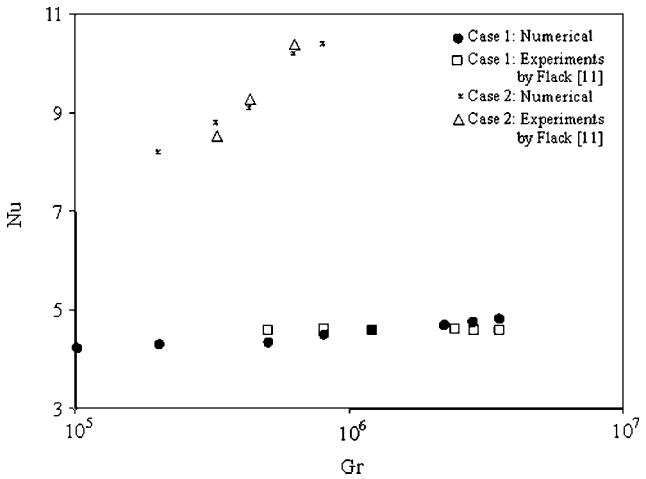

Figure 3. Comparison between the numerical and experimental mean Nusselt numbers for the isosceles triangular cavity: Case 1 (cavity heated from the top) and Case 2 (cavity heated from below).

Convergence of all numerical simulations was assessed in two stages: first, through the monitoring of computed residuals for the mass, velocity, and energy conservation by setting its variations to less than 10^{-6}. Second, through the convergence of point and/or surface monitors for velocity, temperature, and heat flux at selected locations in the computational domain.

Once the velocity and temperature fields $u(x, y)$, $v(x, y)$ and $T(x, y)$ have accurately converged, we proceeded to calculate the streamlines and isotherms to characterize the circulatory airflow. Thereafter, the local heat flux distribution $q_w(x)$ was computed along the lower plate by applying Fourier's law to the temperature distribution $T(x, 0)$, and then integrated over the entire surface. This gives way to the total heat transfer rate:

$$\overline{q_w} = \frac{\int_{\text{base}} q_w(x)\,\mathrm{d}x}{L} \tag{5}$$

From here, the mean convective coefficient in dimensionless form or the mean Nusselt number was determined by

$$Nu = \frac{\overline{q_w}}{T_H - T_C}\left(\frac{H}{k}\right) \tag{6}$$

where k the thermal conductivity of air is evaluated at the reference temperature T_r cited before.

In the course of the numerical computations, the validation of the numerical code was carefully done for the limiting case with $d = 0$ related to the isosceles triangular cavity. The experimental measurements by Flack [11] seemed to be the logical choice. In this work, two heating/cooling conditions corresponding to an isosceles triangular cavity heated from above (Case 1) and heated from below (Case 2) were assessed. Figure 3 illustrates the excellent parity between the collection of experimental and numerical Nusselt numbers Nu varying with the Grashof number for $Pr = 0.7$. From the plot on Figure 3, it may be inferred that Nu stays uniform around 4.63 in Case 1. The invariance of Nu with Gr clearly indicates that the majority of the heat is transported by conduction.

DOI: 10.1002/fld

In contrast, for Case 2, the curve path exhibits a power law dependence of *Nu* with respect to *Gr*; this is responsive to strong natural convection. Among all the *Nu–Gr* data points gathered for the two contrasting cases regardless of the source, the maximum deviation detected is within a tolerable 3.5% band.

4. DISCUSSION OF THE NUMERICAL RESULTS

Air motion was set up in the modified RB cavity by heating the bottom horizontal plate to a uniform temperature T_H and cooling the two symmetric upper inverted-V plates to a uniform temperature T_C. The inclination of the inverted-V plates was expressed by means of the relative heights d of the insulated sidewalls varying from a minimum limit $d=0$, to 0.125, 0.25, 0.5 ending at the maximum limit $d=1$ (standard RB cavity). The Prandtl number of air was set at 0.71, and the Rayleigh number values were assigned inside the large interval extending between 10^3 and 10^6. Naturally, the local quantities to be computed are the air velocity fields $u(x, y)$, $v(x, y)$ and the companion temperature fields $T(x, y)$. The latter was channelled through the global quantity of interest, the mean heat transfer coefficient. The air velocities are provided in terms of adequate streamlines, whereas the temperatures are reported in terms of isotherms. For all cases investigated, we started the computations from rest at low $Ra=10^3$ and use the resulting steady state to start the computations at higher Rayleigh numbers.

In the case of an isosceles triangular cavity ($d=0$) heated from below and evenly cooled from above, it has been demonstrated experimentally by Holtzman *et al*. [12] that multiple steady-state solutions can be obtained in the range of Rayleigh considered in the present work, i.e. $10^3 \leqslant Ra \leqslant 10^6$. Symmetrical steady-state solutions are observed at low Rayleigh numbers, which are characterized by two counter-rotating cells. As *Ra* progressively increased, a transition to an asymmetrical steady state occurs at a critical value of Rayleigh number. Multiple steady-state solutions can also be obtained in the ranges of parameters considered in the present work. A special effort is made in this regard to determine the existing ranges of each steady-state solution as well as the critical values of *Ra* characterizing the transition from one solution to another.

4.1. Fluid flow

The collection of streamlines and isotherms related to a low $Ra=10^3$ is presented in Figure 4. The fluid system is placed slightly above the critical state, which corresponds to the onset of thermal convection. The results are reported for the three RB cavities with $d=0.125, 0.5$, and 1. The steady-state patterns for the three geometries are characterized by two counter-rotating vortices. It is observable that this solution is symmetric about the vertical mid-plane of the modified RB cavity. The buoyant convective motion is oriented upwards in the central region (hot stream) and downwards near the sidewalls (cold stream). The strength of the vortices rotation can be determined by calculating the magnitude of the stream function gradient. The $d=0.125$ cavity displays the largest magnitude for the stream function gradient, while the rectangle ($d=1$) displays the smallest. Therefore, as expected the vortices strength and velocities reach highest values for $d=0.125$ and lowest values for the rectangle ($d=1$). The isotherms specified the typical temperature distribution that corresponds to the limit dictated by pure conduction. For the geometries with $d<1$, the isotherms are parallel to the base plate in the lower region of the cavity but their shape is changing and become parallel to the inclined plate when moving up towards the upper region of the cavity.

DOI: 10.1002/fld

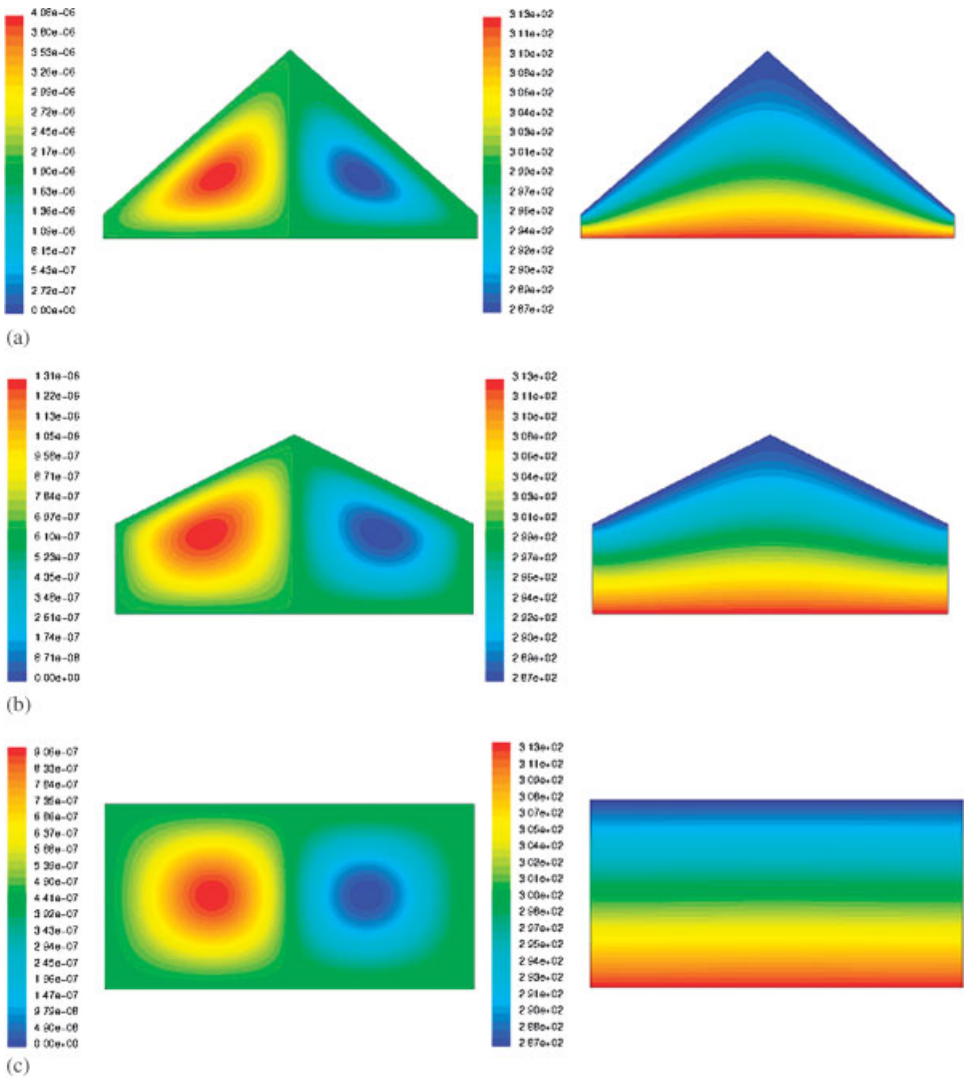

Figure 4. Streamlines and isotherms for a fixed $Ra = 10^3$ and different relative heights: (a) $d = 0.125$; (b) $d = 0.5$; and (c) $d = 1$.

In contrast, for the rectangle the isotherms are horizontal and parallel to the pair of active plates. As demonstrated in Figure 5, the circulation patterns are radically changed for the cavities with $d < 1$ and the symmetry between the two counter-rotating vortices disappeared when Ra increased to 10^6. Further, at this juncture, it is worth noting the presence of a pitchfork bifurcation in Figure 5. This bifurcation occurs at a critical Rayleigh number, Ra_1, which depends upon the height d of the insulated walls. Secondary vortices appear at the corners of the cavity associated with $d = 0.125$ as evidenced in Figure 5(a). These new vortices push the main vortices towards the center and contribute to intensify the heat transfer across the cavity. However, when increasing Ra from 10^3

DOI: 10.1002/fld

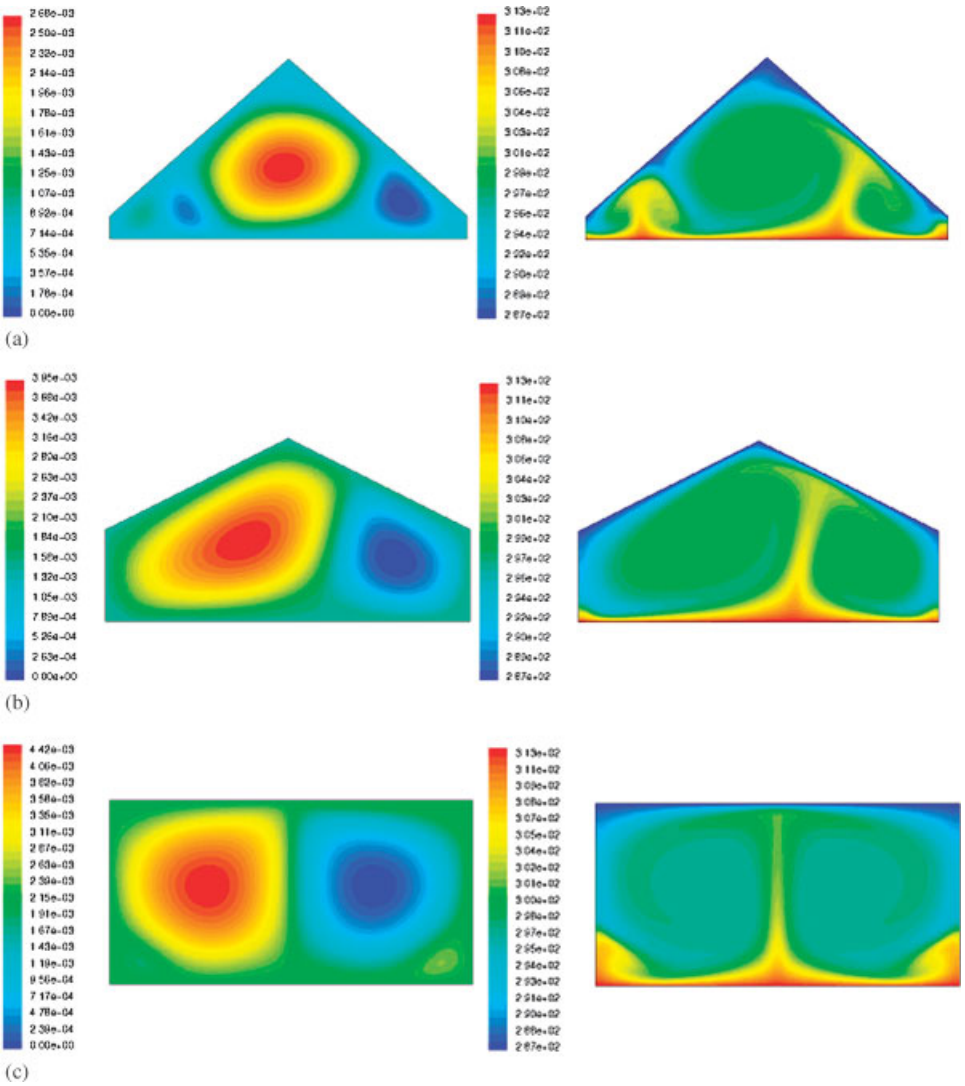

Figure 5. Streamlines and isotherms for a fixed $Ra = 10^6$ and different relative heights in a modified RB cavity with: (a) $d = 0.125$; (b) $d = 0.5$; and (c) $d = 1$.

in the intermediate cavity with $d = 0.5$, one cell amplifies in size and moves from the corner towards the center while the second cell remains in the corner but diminishes in size. Contrary to the compartment exhibited by the first two geometries, the airflow stays symmetrical with respect to the mid-plane for the rectangle. Essentially, the airflow exhibits the same two original vortices, plus two small secondary vortices that surface up in the lower corners. In addition to the new vortex locations, their strengths are also intensified as seen by the magnitude of the stream function gradient. The effect of the enhanced vortex strengths can be elucidated in the temperature contours,

DOI: 10.1002/fld

which in fact become complex. The difference in the isotherm shapes highlights the importance of buoyant convection over conduction at a particular Rayleigh number.

4.2. Transition

The buoyant air motion is steady for a wide range of Ra, but as Ra was gradually increased, the symmetric (S) patterns disappear and a sub-critical pitchfork bifurcation is created at a critical value of Rayleigh number, say Ra_1. Above this Ra_1 threshold the asymmetric (AS) patterns appear, remaining steady for a wide range of Ra. This state of affairs prevails even if the initial conditions imposed on the air are those of the symmetrical flow. Special effort has been devoted to determine the critical Rayleigh number Ra_1 characterizing the transition from the S steady-state solution to an AS steady-state solution for different heights d of the insulated sidewalls. Tests were conducted by increasing Ra, with very small steps when necessary (as low as $\Delta Ra = 10$), to determine these critical values. All transitions were determined with a precision such that $\Delta Ra < 10$ from the critical values examined. The computed Ra_1 results *versus* d may be conveniently viewed when plotting them on a phase diagram that shows the existence ranges of each solution. The resulting diagram is illustrated in Figure 6. The S-flow exists under the curved line, characterizing the variations of Ra_1 over a limited range of Ra and d. Meanwhile, the AS flow exists for a wide domain of the diagram, which corresponds to high Rayleigh numbers.

At this stage, we express interest in measuring the degree of asymmetry in the numerical-determined temperature solutions. To accomplish this objective the following integral I is evaluated

$$I = \frac{\int [T(x, y) - T(-x, y)]^2 \, dx \, dy}{4 \int [T(x, y)]^2 \, dx \, dy} \tag{7}$$

over the whole geometry: from this formal definition, it is clear that the S steady-state solution satisfies $I = 0$, but the AS steady-state solution has a nonzero I. The quantity I has been

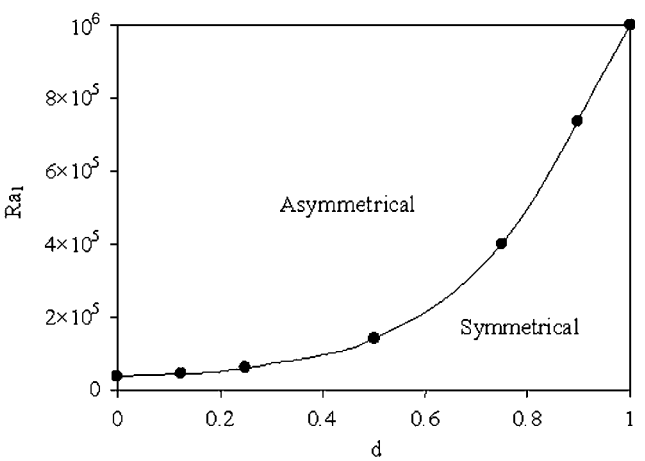

Figure 6. Phase diagram relative to the existence of the two solutions for different combinations of Ra and d in a modified RB cavity.

DOI: 10.1002/fld

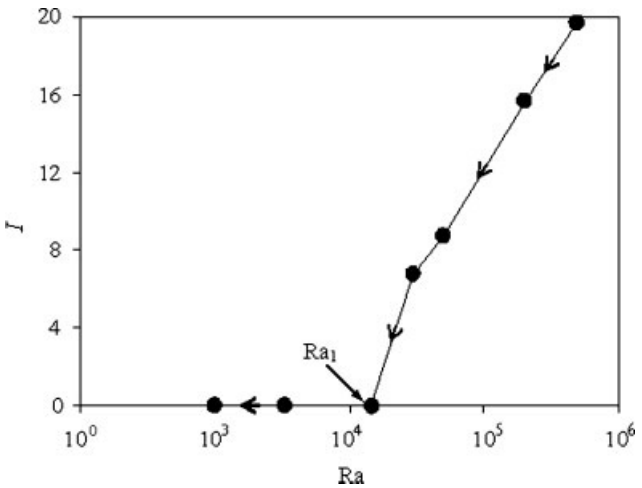

Figure 7. Evolution of the degree of symmetry I with the Rayleigh number for a modified RB cavity with $d = 0.125$.

evaluated in the case of $d = 0.125$ for different Ra ranging from 10^3 up to 5×10^5. The outcome of these calculations is displayed in Figure 7 when decreasing Ra from 5×10^5 to a final 10^3. It may be seen that I decay monotonically with Ra as the main plume approaches the mid-plane of the cavity. This singular behavior continues steadily until Ra reaches the critical value Ra_1 where I becomes zero.

4.3. Heat transfer

Displayed in Figure 8 are local heat flux distributions for $Ra = 10^5$. The local heat flux results correspond to the three configurations: $d = 0, 0.125$, and 0.75. For the isosceles triangle ($d = 0$) q_w begins with a large value at the point where the discontinuity $X = 0$ occurs. As X grows, q_w possesses a positive skewed concave U-shape with respect to the abscissa X. In the sub interval $0.1 \leqslant X \leqslant 0.9$ q_w stays almost constant showing subtle variations characterized by the presence of peaks. Each peak is the direct result of an upward air stream between two rotating vortices. The magnitude of each peak is proportional to the strength of the corresponding vortex. Approaching the other $X = 1$ discontinuity, q_w magnifies quickly to reach high values indicating that heat transfer by conduction has happened in this region. The effect of the insulated sidewalls on the local heat flux can be seen on the first q_w curve representative of the $d = 0.125$ cavity. The value of q_w at the extremes $X = 0$ and 1 descends 10-fold from 1500 to 150 $\mathrm{W\,m^{-2}}$. Besides the values of q_w at the discontinuity, q_w curve exhibits the same behavior as noticed by q_w corresponding to the isosceles cavity ($d = 0$). In addition, it is worth mentioning here that the presence of the small, insulated sidewalls provides a huge heat transfer enhancement in the modified RB cavity.

The mean Nusselt number Nu as a function of the log Ra and parameterized by the relative height d of the insulated sidewalls is plotted in Figure 9. Regarding the lowermost Nu curve representative of the rectangular cavity ($d = 1$), this particular curve constitutes the standard RB cavity. This is taken here as the benchmark solution for comparison purposes. The response of Nu to changes in Ra may be viewed as the intersection of two straight lines, one horizontal

DOI: 10.1002/fld

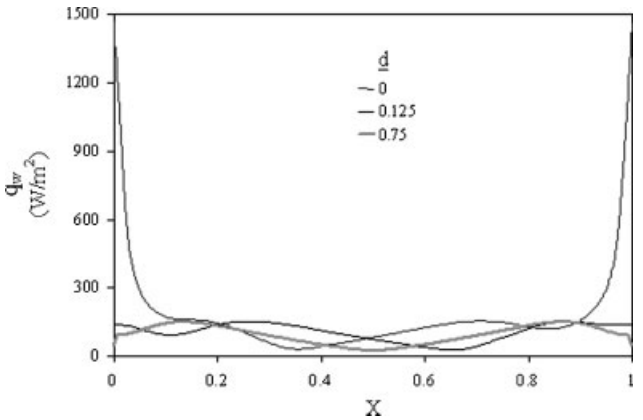

Figure 8. Distribution of the local heat flux q_w along the hot bottom plate for a fixed $Ra = 10^5$ and various heights d in a modified RB cavity.

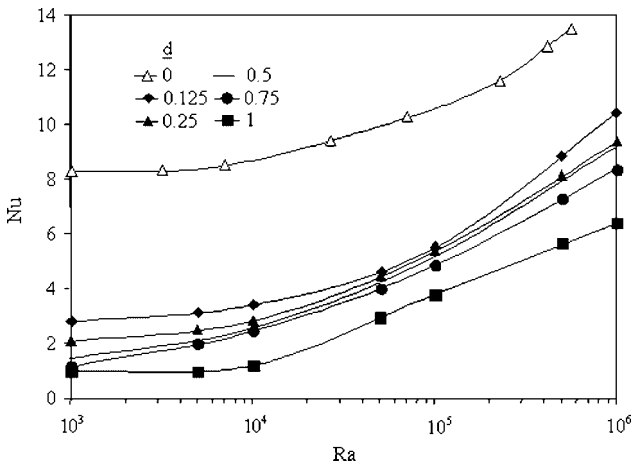

Figure 9. Variation of the mean Nusselt number Nu with the Rayleigh number Ra and the relative height d of the insulated sidewalls in several modified RB cavities.

and the other with a positive slope. The point where the curves start losing their horizontal path can be viewed as the critical value of Ra_C, which is associated with the relative height d. The significance of the critical value is important because it serves to identify the onset of natural convection. Basically, at small values of Ra below the critical value, there is little augmentation in the heat transfer over that due to conduction. The conduction regime is described by a linear temperature variation in the central region of the geometry. As Ra increases, the airflow regimes include conduction, transition, and boundary layer; this results in a significant augmentation in convection heat transfer. Upon reduction of the insulated sidewalls height to $d = 0.75$, the shape of the Nu curve straighten up and is shifted up slightly by one unit at a low $Ra = 5 \times 10^3$ and two units at a high $Ra = 10^6$. When the height of the insulated sidewalls is changed markedly from

DOI: 10.1002/fld

$d = 0.75$ to 0.125, each different height gives rise to Nu curves that are nearly parallel. For this geometry sub-group forming modified RB cavities, remarkable heat transfer enhancements were observed when compared against the standard RB cavity with $d = 1$. The largest heat transfer enhancement takes place between the standard RB cavity with $d = 1$ and the modified RB cavity with $d = 0$. First, an increment of the order of $\Delta Nu = 8$ units, equivalent to 700% is observed for a low $Ra = 10^3$. Second, for a high $Ra = 6 \times 10^5$, the increment ascends to $\Delta Nu = 8$ units, equivalent to 145%.

A nonlinear multiple regression analysis was carried out with the numerical-generated data for the mean Nusselt number for suitable combinations of Rayleigh numbers and the relative height of insulated sidewalls d. At the end, it was decided to recommend the predictive correlation equation

$$\begin{aligned} Nu = {} & 8.4198 - 78.1417d + 350.5906d^2 - 741.9289d^3 + 726.0692d^4 - 264.2173d^5 \\ & + 2.7031 \times 10^{-5} Ra - 7.7931 \times 10^{-11} Ra^2 + 1.1294 \times 10^{-16} Ra^3 - 5.4795 \times 10^{-23} Ra^4 \\ & + 2.4447 \times 10^{-4} d \times Ra - 2.0125 \times 10^{-9} d \times Ra^2 + 2.0746 \times 10^{-15} d \times Ra^3 \\ & - 3.0193 \times 10^{-22} d \times Ra^4 - 8.4759 \times 10^{-5} d^2 \times Ra + 3.7320 \times 10^{-10} d^2 \times Ra^2 \\ & - 6.6865 \times 10^{-16} d^2 \times Ra^3 + 3.7386 \times 10^{-22} d^2 \times Ra^4 \end{aligned} \tag{8}$$

The nearly perfect R^2 value of 99.7% means that 99.7% of the variability in Nu caused by changes in d and Ra can be explained by the 18 predictor variables in Equation (8). The range of validity of Equation (8) is $0 \leqslant d \leqslant 1$ and $10^3 \leqslant Ra \leqslant 10^6$. The maximum error that results between the numerical and the predicted Nu is less than 10%.

5. CONCLUDING REMARKS

Laminar heat transfer and fluid flow of air inside a modified Rayleigh–Bénard (RB) cavity is investigated. The cavity domain is bounded from below by a flat plate and from above by an inverted-V plate with variable inclination angles. Flow patterns of the modified RB cavity are found to be symmetrical at low Ra, but as Ra was gradually increased above a critical value Ra_1, a transition to asymmetrical patterns occurs. The critical value increases with the height d of the insulated sidewalls. Local and mean heat fluxes throughout the active walls of the cavity are highly affected by the height d of the sidewalls and this effect is intensified as d decreases. In fact, when d decreases from 0.125 to 0, increment in terms of the mean Nusselt number of up to 63.4% at low Rayleigh number and 33.3% at high Rayleigh number was obtained. These two increment values go up to 700 and 145%, respectively, when d is reduced from 1 to 0. A generalized correlation equation for the mean Nusselt number is proposed. This correlation equation allows accurate predictions for the entire ranges of the Rayleigh number and the dimensionless height of the vertical sidewalls considered.

NOMENCLATURE

c_p	specific isobaric heat capacity ($\mathrm{J\,kg^{-1}\,K^{-1}}$)
d	relative height of insulated sidewalls $= d'/H$
d'	height of insulated sidewalls (m)

DOI: 10.1002/fld

g	acceleration of gravity ($m\,s^{-2}$)
h	mean convective coefficient ($W\,K^{-1}\,m^{-2}$)
H	maximum height of RB cavity (m)
k	thermal conductivity ($W\,K^{-1}\,m^{-1}$)
L	base of the RB cavity (m)
Nu	mean Nusselt number $= hH/k$
p	pressure (Pa)
q_w	wall heat flux ($W\,m^{-2}$)
$\overline{q_w}$	mean wall heat flux ($W\,m^{-2}$)
Ra	Rayleigh number $= g\beta(T_H - T_C)H^3/\alpha v$
T	temperature (K)
T_C	cold plate temperature (K)
T_H	hot plate temperature (K)
T_r	reference temperature $= (T_H + T_C)/2$
u, v	velocities in the x- and y-directions ($m\,s^{-1}$)
x, y	horizontal and vertical coordinates (m)
X, Y	dimensionless x, y; $x/L, y/L$

Greek letters

α	thermal diffusivity ($m^2\,s^{-1}$)
β	volumetric thermal expansion coefficient (K^{-1})
μ	dynamic viscosity ($kg\,m^{-1}\,s^{-1}$)
v	kinematic viscosity ($m^2\,s^{-1}$)
ρ	density ($kg\,m^{-3}$)
ψ	stream function $u = \partial\psi/\partial y$, $v = -\partial\psi/\partial x$

REFERENCES

1. Jaluria Y. Natural convection. In *Heat Transfer Handbook*, Chapter 7, Bejan A, Kraus AD (eds). Wiley: New York, 2003.
2. Raithby GD, Hollands KGT. Natural Convection, In *Handbook of Heat Transfer*, Chapter 4 (3rd edn), Rohsenow WP, Hartnett JP, Cho YI (eds). McGraw-Hill: New York, 1998.
3. Bénard H. Les tourbillons cellulaires dans une nappe liquide transportant de la chaleur par convection en régime permanent. *Annales de Chimie et de Physique* 1900; **23**:62–144.
4. Hitt DL, Campo A. Influence of transverse fins attached to the heated plate of a Rayleigh–Bénard cavity. *Proceedings of the IMECE ASME Conference*, Anaheim, CA, November 2004.
5. Lam SW, Gani R, Symons JG. Experimental and numerical studies of natural convection in trapezoidal cavities. *Journal of Heat Transfer* (ASME) 1989; **111**:372–377.
6. Peric M. Natural convection in trapezoidal cavities. *Numerical Heat Transfer*, *Part B* 1993; **24**:213–219.
7. Sadat H, Salagnac P. Further results for laminar natural convection in a two-dimensional trapezoidal enclosure. *Numerical Heat Transfer*, *Part A* 1995; **27**:451–459.
8. Moukalled F, Acharya S. Buoyancy-induced heat transfer in partially divided trapezoidal cavities. *Numerical Heat Transfer*, *Part A* 1997; **32**:787–810.
9. Moukalled F, Acharya S. Natural convection in trapezoidal cavities with baffles mounted on the upper inclined surfaces. *Numerical Heat Transfer*, *Part A* 2000; **37**:545–565.
10. Patankar SV. *Numerical Heat Transfer and Fluid Flow*. Hemisphere, McGraw-Hill: New York, 1980.
11. Flack RD. The experimental measurement of natural convection heat transfer in triangular enclosures heated or cooled from below. *Journal of Heat Transfer* (ASME) 1980; **102**:770–772.
12. Holtzman GA, Hill RW, Ball KS. Laminar natural convection in isosceles triangular enclosures heated from below and symmetrically cooled from above. *Journal of Heat Transfer* 2000; **122**:485–491.

DOI: 10.1002/fld